NANO LETTERS

Letter

pubs.acs.org/NanoLett

High Ionic Conductivity of Composite Solid Polymer Electrolyte via In Situ Synthesis of Monodispersed SiO_2 Nanospheres in Poly(ethylene oxide)

Dingchang Lin,[†] Wei Liu,[†] Yayuan Liu,[†] Hye Ryoung Lee,[‡] Po-Chun Hsu,[†] Kai Liu,[†] and Yi Cui*[,†,§]

[†]Department of Materials Science and Engineering and [‡]Department of Electrical Engineering, Stanford University, Stanford, California 94305, United States

[§]Stanford Institute for Materials and Energy Sciences, SLAC National Accelerator Laboratory, 2575 Sand Hill Road, Menlo Park, California 94025, United States

Supporting Information

ABSTRACT: High ionic conductivity solid polymer electrolyte (SPE) has long been desired for the next generation high energy and safe rechargeable lithium batteries. Among all of the SPEs, composite polymer electrolyte (CPE) with ceramic fillers has garnered great interest due to the enhancement of ionic conductivity. However, the high degree of polymer crystallinity, agglomeration of ceramic fillers, and weak polymer−ceramic interaction limit the further improvement of ionic conductivity. Different from the existing methods of blending preformed ceramic particles with polymers, here we introduce an in situ synthesis of ceramic filler particles in polymer electrolyte. Much stronger chemical/mechanical interactions between monodispersed 12 nm diameter SiO_2 nanospheres and poly(ethylene oxide) (PEO) chains were produced by in situ hydrolysis, which significantly suppresses the crystallization of PEO and thus facilitates polymer segmental motion for ionic conduction. In addition, an improved degree of $LiClO_4$ dissociation can also be achieved. All of these lead to good ionic conductivity (1.2×10^{-3} S cm^{-1} at 60 °C, 4.4×10^{-5} S cm^{-1} at 30 °C). At the same time, largely extended electrochemical stability window up to 5.5 V can be observed. We further demonstrated all-solid-state lithium batteries showing excellent rate capability as well as good cycling performance.

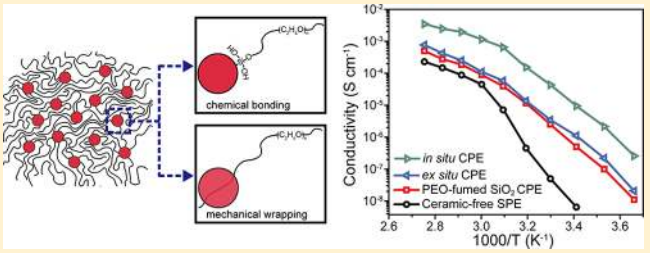

KEYWORDS: *Solid composite polymer electrolyte, in situ synthesis, silica nanosphere, poly(ethylene oxide), ionic conductivity*

Lithium ion batteries (LIB) have gained great commercial success as the leading power source for consumer electronics and electric vehicles.[1,2] LIB currently uses liquid organic electrolyte, which however has a main issue of flammability.[3,4] In addition, the demand of high energy density batteries has driven the development of novel electrode materials such as high capacity Si and Li metal anodes,[5−11] high voltage oxide,[12] and high capacity sulfur cathodes.[13,14] For these new materials, liquid electrolytes present challenging issues such as uncontrolled side chemical reactions, Li dendrite formation, and polysulfide dissolution. Exploring solid electrolyte can result in promising solutions to all of the above problems.[15−25] Particularly, solid polymer electrolytes (SPE) can afford an attractive approach.[17−19] Their good mechanical strength can effectively mitigate dendrite penetration,[26−28] while the potentially high electrochemical stability enables the stable operation of batteries at extended voltage window.[3,19,29] The solid state nature can prevent polysulfide dissolution. Furthermore, the excellent processability, flexibility, and low flammability open up the opportunity for the fabrication of high packing efficiency, flexible, and safe batteries.[3,4]

Despite the numerous advantages, the use of SPE is severely impeded by its relatively low ionic conductivity (10^{-6}−10^{-8} S cm^{-1} at room temperature for polymer-Li salt blends). It is generally believed that the ionic conductivity of SPE is mainly contributed by the amorphous regions; therefore, the inherently high degree of polymer crystallinity seriously limits the ion transport.[17−19] The addition of plasticizers to form gel polymer electrolyte (GPE) can significantly improve the ionic conductivity,[30−33] but only with the sacrifice of the principal benefits of SPE, including the mechanical strength, electrochemical stability, and low flammability. To develop dried solid polymer electrolytes without plasticizer, several alternative strategies, such as forming block copolymer,[34−39] aligning polymer chains,[16,40−42] cross-linking polymers with metal alkoxides,[43−45] and adding ceramic fillers[15,46−54] have been extensively studied. Of these alternates, the incorporation of ceramic fillers has attracted considerable attention due to the remarkably improved ionic conductivity, high mechanical

Received: October 9, 2015
Revised: November 19, 2015
Published: November 23, 2015

DOI: 10.1021/acs.nanolett.5b04117
Nano Lett. 2016, 16, 459−465

strength, and simplified fabrication procedures. Two hypotheses regarding the mechanism of ionic conductivity improvement by ceramic fillers have been proposed and demonstrated.[49,55,56] First, the ceramic fillers perform as cross-linking centers to reduce the polymer crystallinity, facilitating the segmental motion. Second, the strong Lewis acid−base interaction between electrolyte ion species and the surface chemical groups of ceramic fillers can enhance salt dissociation and stabilize the anions. The existing methods to prepare ceramic-polymer composite electrolyte are through mixing preformed ceramic particles with polymers. However, considerable amount of crystallized polymer regions still exist, together with the agglomeration of ceramic fillers and the relatively weak polymer−ceramic interaction, making the further improvement of ionic conductivity a challenge.

Herein, we report a new method to prepare ceramic−polymer electrolyte via in situ synthesis ceramic particles inside polymer electrolyte. As a demonstration, we developed the poly(ethylene oxide) (PEO)−monodispersed ultrafine SiO_2 ($MUSiO_2$) composite polymer electrolyte (PEO-$MUSiO_2$ CPE) via in situ hydrolysis of tetraethyl orthosilicate(TEOS) in PEO solution. The strong chemical/mechanical interactions between $MUSiO_2$ spheres and PEO chains formed during the in situ synthesis, successfully suppressed the degree of PEO crystallinity. Moreover, since precisely controlled growth of SiO_2 is applied, better particle distribution and monodispersity can be achieved, which enhance the effective surface area for efficient Lewis acid−base interaction. With all the benefits of the well-controlled in situ synthesis, the ionic conductivity of PEO-$MUSiO_2$ CPE is considerably improved compared to the ceramic filler-free PEO and even 1 order of magnitude higher than its counterpart by simple mechanical mixing. The electrochemical stability window is also largely extended. Over 5.5 V versus Li^+/Li of voltage can be endured without significant anodic decomposition. Thanks to the excellent CPE developed here, we further demonstrate the all-solid-state lithium batteries with good rate capability and stable cycling performance. When operating under 1C, around 120 mAh g^{-1} and 100 mAh g^{-1} of capacity of $LiFePO_4$ can be retained at 90 and 60 °C, respectively, and no significant capacity decay can be observed within 80 cycles.

Figure 1 schematically shows the synthesis of in situ hydrolyzed PEO-$MUSiO_2$ CPE (in situ CPE). To obtain PEO-$MUSiO_2$ composites with ∼12 nm SiO_2, crystalline PEO, as the starting materials, was first dissolved in deionized water to afford a diluted solution. After tuning the pH of the solution to ∼10.4 with ammonia, TEOS was added dropwise into the system to initiate the hydrolysis reaction. Since no cosolvent was used in this system, TEOS and the aqueous solution were phase-separated. This two-phase hydrolysis of TEOS is known to be critical for the precise size control of $MUSiO_2$ spheres by slowly delivering hydrolyzed TEOS into the aqueous phase.[57,58] PEO-$MUSiO_2$ composites with larger SiO_2 size (∼30 nm and ∼45 nm) were synthesized based on the regrowth technique with ∼12 nm SiO_2 spheres as seeds.[59] Unless specified otherwise, the weight percentage of SiO_2 in CPEs was controlled to be ∼10%. When hydrolysis was complete, dehydrated $LiClO_4$ salt was added to fix the EO−Li^+ ratio at 8:1. Afterward, ∼ 200 μm of solid electrolyte membranes were attained by doctor blading the SPE on polytetrafluoroethylene (PTFE) plates. The as-obtained laminates were then dried at 60 °C in vacuum oven for 24 h and stored in an argon-filled glovebox for at least 48 h before measurement to guarantee the removal of trace amount of water.

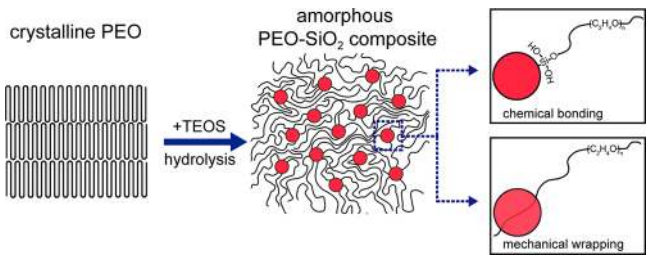

Figure 1. Schematic figures showing the procedure of in situ hydrolysis and interaction mechanisms among PEO chains and $MUSiO_2$. Starting with pure crystalline PEO, after in situ hydrolysis we can form strongly interacting PEO -$MUSiO_2$ composite with almost amorphous PEO. Two possible interaction mechanisms are shown including chemical bonding between the ends of PEO chains with hydroxyl groups on $MUSiO_2$ surfaces and mechanical wrapping of PEO chains during the growth of $MUSiO_2$ spheres.

The in situ hydrolysis offers the opportunities to form much stronger interaction between polymer chains and SiO_2 nanospheres, which is crucial for decreasing polymer crystallinity. It was reported that alkoxysilane can efficiently cross-link PEO into infinite network.[43−45] Here, rather than cross-linking the PEO into a network, we take advantage of the chemical bonding between alkoxysilane and PEO to strongly link PEO chains onto SiO_2 nanospheres, which can be achieved by in situ hydrolysis of TEOS with the presence of PEO. The in situ hydrolysis creates two possible strong interaction mechanisms between SiO_2 and PEO chains, namely, chemical bonding and mechanical wrapping, which can highly reduce the PEO crystallinity. As shown schematically in Figure 1, on one hand, the hydroxyl groups at the ends of PEO chains can chemically bind with those on SiO_2 surface under hydrolysis condition, and on the other hand, when the SiO_2 spheres grows, the PEO chains can be mechanically wrapped and partially embedded inside SiO_2 spheres. These two possible interaction mechanisms can pin the polymer chains locally and prevent their crystallization.

Transmission electron microscopy (TEM) was utilized to characterize the as-synthesized PEO-$MUSiO_2$ composites by in situ hydrolysis with different SiO_2 sizes (Figure 2a−f). PEO was stained with 0.1% phosphotungstic acid for better contrast. As can be observed from the images, high monodispersity can be achieved for SiO_2 of all sizes from ∼12 nm to ∼45 nm. When compared to the corresponding scanning electron microscopy (SEM) images (Figure 2g−i, Supplementary Figure S1) of their counterparts synthesized without PEO, the size and monodispersity of the nanospheres are similar, indicating the consistency of SiO_2 synthesis with and without the presence of PEO. In addition, it is clearly illustrated in the magnified TEM images (Figure 2d−f) that a darker-colored layer exists around every SiO_2 sphere. When compared the TEM images of in situ synthesized composite with the ex situ counterparts (Supplementary Figure S9), it is clear that much darker shells can be observed in in situ synthesized composite. Since the darker regions of stained PEO indicate higher polymer density, it suggests the strong interaction between SiO_2 and PEO chains on surface. In Figure 2j, X-ray diffraction (XRD) spectra of different compositions are compared to show the crystallinity under different conditions. All of the spectra were measured at ambient temperature based on the same area and thickness of

DOI: 10.1021/acs.nanolett.5b04117
Nano Lett. 2016, 16, 459−465

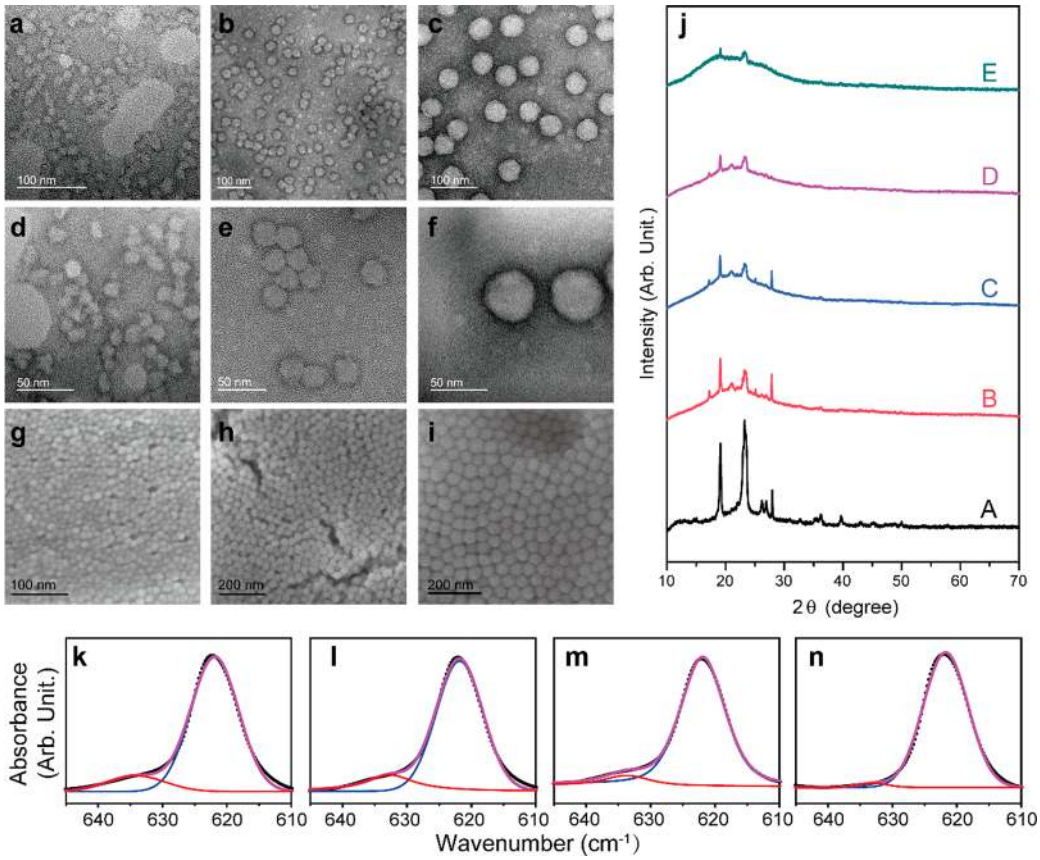

Figure 2. Characterizations of in situ CPE. (a–f) TEM images of in situ PEO-$MUSiO_2$ composite with different sizes of ~12 nm (a, d), ~ 30 nm (b, e), and ~45 nm (c, f). PEO was stained with 0.1% phosphotungstic acid to show better contrast. (g–i) SEM images of as-synthesized corresponding $MUSiO_2$ spheres (without PEO) with various sizes of ~12 nm (g), ~ 30 nm (h), and ~45 nm (i). (j) Comparison on XRD spectra of pure PEO (A), ceramic-free SPE (B), PEO-fumed SiO_2 CPE (C), ex situ CPE (D), and in situ CPE (E). (k–n) FT-IR spectra at 610–645 cm^{-1} and corresponding Gaussian–Lorentzian fitting of the ClO_4^- absorbance for ceramic-free PEO SPE (k), PEO-fumed SiO_2 CPE (l), ex situ CPE (m), and in situ CPE (n).

samples for fair comparison. Curve A, which is the spectrum of pure PEO, shows strong characteristic peaks of crystalline PEO, indicating the high tendency of PEO to crystallize at ambient temperature. A dramatic drop on peak intensity can be observed with the addition of $LiClO_4$ salt (curve B), which implies that $LiClO_4$ salt can reduce the crystallinity of PEO. Nevertheless, a considerable level of crystalline phase can still be observed. The incorporation of 10% fumed SiO_2 (PEO-fumed SiO_2 CPE, curve C) or ex situ synthesized $MUSiO_2$ (ex situ CPE, curve D) show further decrease in peak intensity, with the latter being more effective. This difference can be attributed to the smaller average size (~12 nm) and the higher degree monodispersity of the $MUSiO_2$ compared to the fumed SiO_2 counterpart (~14 nm). Notably, the PEO-$MUSiO_2$ composite by in situ synthesis (curve E) shows almost indiscernible peaks, with only two very weak signals, indicating the lowest degree of crystallinity. In addition, the intensity of the amorphous halo at $2\theta \sim 20–30°$ is increased accordingly from curve A to E with E having the highest intensity of amorphous halo. This trend in crystallinity is further confirmed with Fourier transform infrared spectroscopy (FT-IR) spectra (Supplementary Figure S4) and differential scanning calorimetry (DSC) analysis (Supplementary Figure S6), where the in situ PEO-$MUSiO_2$ composite has the weakest absorbance intensity in FT-IR spectrum and lowest endothermic peak in DSC spectrum, indicating higher fraction of amorphous phase.

All of the evidence indicates that much more amorphous PEO can be obtained by the in situ hydrolysis, which is crucial for ionic conductivity improvement. Two reasons can be attributed to the low crystallinity. First, the above-mentioned strong interactions between $MUSiO_2$ spheres and polymer chains can efficiently pin the polymer chains and prevent their reorganization, which can keep the low crystallinity state of the PEO. Second, $MUSiO_2$ spheres from in situ hydrolysis are more uniform in size and much more evenly distributed inside the PEO matrix. This highly improves the effective surface area of SiO_2 and thus the interactions among SiO_2, polymer chains, and the ionic species.

In addition to the degree of crystallinity, the dissociation of $LiClO_4$ in PEO is also critical for good ionic conductivity, which can be strongly affected by the interactions among PEO, $LiClO_4$, and SiO_2. According to the previous studies,[60–62] FT-IR spectra with wavenumber in the range of 610–650 cm^{-1} directly reveals the dissociation of $LiClO_4$. Specifically, the peak at ~624 cm^{-1} is assigned to the dissociated free anion and the other at ~635 cm^{-1} corresponds to the bonded ion pair. Figure 2k–n shows the spectra and the corresponding Gaussian–Lorentzian fitting results of the ceramic free SPE (k), PEO-fumed SiO_2 CPE (l), ex situ CPE (m), and in situ CPE (n). As is shown, the peak area ratio of free anion versus bonded ion pair increases from left to right, which indicates that the degree of dissociation enhances accordingly. The simulated dissocia-

DOI: 10.1021/acs.nanolett.5b04117
Nano Lett. 2016, 16, 459–465

tion ratios were summarized in Supplementary Table S1. For the in situ CPE, 98.1% of dissociation ratio can be observed, significantly higher the ceramic-free SPE (85.0%), PEO-fumed SiO_2 CPE (87.4%), and ex situ CPE (92.8%) counterparts. This indicates that with in situ hydrolysis technique, we are able to produce PEO matrix with significantly improved capability to dissociate $LiClO_4$ salt. Two factors may be responsible for the high degree of dissociation. First, the SiO_2 with the small size and high monodispersity offers maximized surface area. This further enhances the interactions of ClO_4^- with SiO_2 surface. Second, the decreasing crystallinity of PEO dramatically enhances the segmental motion of polymer chains, which strengthen the binding between Li^+ and ether groups on PEO chains. Both of the factors contribute to the separation of Li^+ and ClO_4^- in PEO matrix.

To evaluate the ionic conductivity of the SPE membranes, cells with symmetric configuration of stainless steel (SS)/SPE/SS were assembled in an argon-filled glovebox with O_2 and H_2O at subppm levels. The well-sealed cells were then transferred to an environmental chamber (BTU-133, ESPEC North America, Inc.) for temperature-dependent AC impedance measurement with the temperature scanned from 0 to 90 °C. For electrochemical stability test of the SPEs, cyclic voltammetry (CV) measurements were performed on Li/SPE/SS cells.

Arrhenius plots of ionic conductivity with temperature varied from 0 to 90 °C are shown in Figure 3a. When compared with that of ceramic-free PEO SPE, significant improvement in ionic conductivity can be observed by mechanically mixing PEO and SiO_2 to form CPE, which is consistent with previously reported results.[15] Notably, the in situ hydrolysis technique showed prominent effect on further facilitating the ion transport. Substantially improved ionic conductivity can be attained via in situ hydrolysis, with approximately ten times higher value compared to the ex situ PEO-$MUSiO_2$ CPE counterparts. At ambient temperature, the ionic conductivity of in situ PEO-$MUSiO_2$ CPE is in the range of 10^{-4}–10^{-5} S cm^{-1}, while at elevated temperature it shows ionic conductivity values (1.2×10^{-3} S cm^{-1} at 60 °C) comparable to liquid electrolyte. We also compared its ionic conductivity at 30 and 60 °C with those reported in literatures with similar components but synthesized by mechanical mixing. As shown in Supplementary Table S2, we can clearly see that the ionic conductivity by in situ synthesis outperforms those by simple mechanical mixing. From 3 times to orders of magnitude higher ionic conductivity can be observed when compared to the typical results by mechanical mixing.

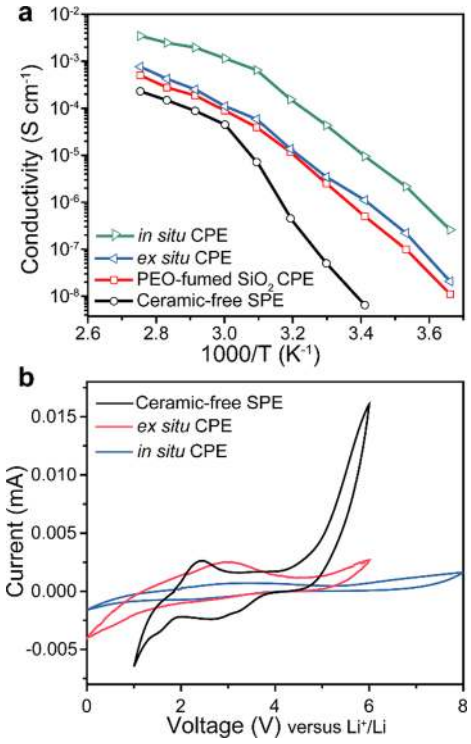

Figure 3. Electrochemical performance of in situ CPE. (a) Arrhenius plots of ionic conductivity of ceramic-free SPE, PEO-fumed SiO_2 CPE, ex situ CPE, and in situ CPE. (b) Electrochemical stability windows of ceramic-free PEO, ex situ CPE, and in situ CPE measured by cyclic voltammetry at 10 mV s^{-1}.

The electrochemical stability window of the electrolyte is critical for high-energy lithium batteries. Recently, many high potential cathode materials have been developed; however, electrolytes that are stable enough to endure anodic decomposition at high potential versus Li^+/Li remain elusive. With in situ hydrolysis, we are able to develop CPE with highly improved electrochemical stability. Here, CV curves of ceramic-free PEO CPE, ex situ CPE, and in situ CPE are shown accordingly with a scan rate of 10 mV s^{-1} (Figure 3b). For ceramic-free PEO electrolyte, it decomposes at a potential ~4.3 V versus Li^+/Li, with small peaks at even lower potential, indicating the instability of the electrolyte. For ex situ CPE, the decomposition potential is slightly higher, at ~4.7 V versus Li^+/Li. Notably, highly extended electrochemical stability window, > 5.5 V can be observed for in situ CPE. It has been studied that the anodic decomposition of anion can be responsible for the electrochemical instability at high potential.[19] The improvement of electrochemical stability indicates that the adsorption effect on anion is much stronger in the in situ CPE, which suppresses its anodic decomposition at high potential.[63]

In the past, operation of all-solid-state cells based on dry solid polymer electrolyte was reported by some works.[38,64–66] Here, with the enhanced ionic conductivity and electrochemical stability, we are able to make all-solid-state lithium polymer batteries and demonstrate highly improved performance. $LiFePO_4$ cathode and lithium metal anode were used to study the cycling performance. To fabricate the electrodes, $LiFePO_4$, PEO-$LiClO_4$ SPE, and carbon black were mixed with the weight ratio of 65:20:15 in acetonitrile to afford slurry with appropriate viscosity before it is coated on Al foil by doctor blading. After drying, calender process was performed to densify the electrodes. Cells were then assembled with the cell configuration of LFP/SPE (~150 μm)/Li foil with neither separator nor liquid electrolyte required. To test the electrochemical performance, galvanostatic cycling were performed between 2.5 and 4.1 V with equivalent charge and discharge rates.

Figure 4a shows the voltage profiles of all-solid-state batteries with in situ CPE under different rates at elevated temperature (90 °C), in which excellent rate capability can be achieved. When running under 1 C (170 mA g^{-1} based on the weight of $LiFePO_4$), the cell shows a high capacity retention of ~120 mAh g^{-1}. Furthermore, flat plateau with low overpotential can be observed, which indicates the fast kinetics of Li^+ transport in CPE. At lower operating temperature (60 °C), good rate capability can still be attained (Figure 4b), with >100 mAh g^{-1} specific capacity retention at 1 C. It is noted that the

DOI: 10.1021/acs.nanolett.5b04117
Nano Lett. 2016, 16, 459–465

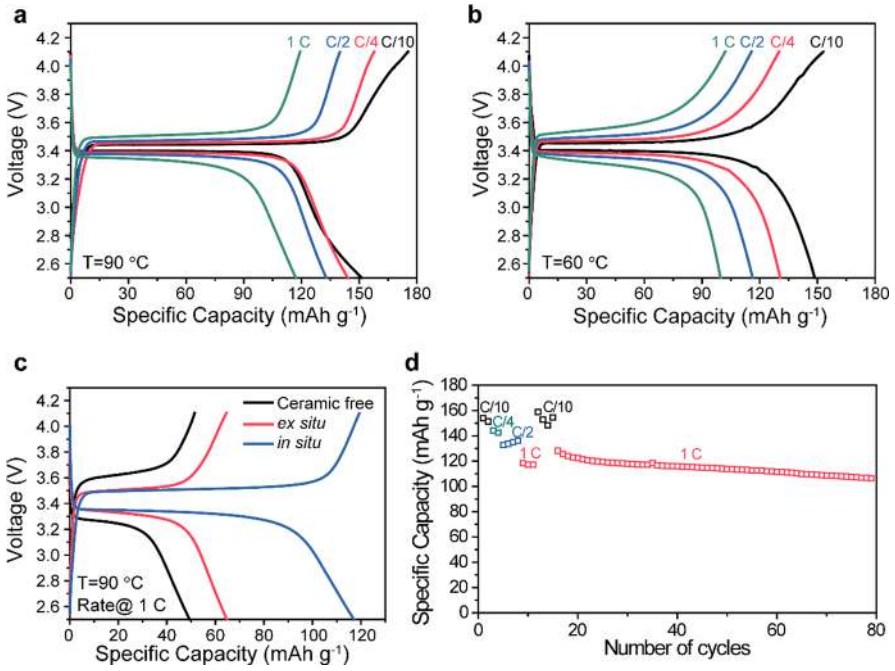

Figure 4. Electrochemical performance of all-solid-state lithium polymer batteries. (a, b) Rate capability of lithium polymer batteries with configuration of $LiFePO_4$ cathode/in situ CPE/lithium foil anode at 90 °C (a) and 60 °C (b). (c) Comparison on capacity retention of batteries with different electrolytes of ceramic-free SPE, ex situ CPE, and in situ CPE operating at 90 °C and the rate of 1 C. (d) Cycle performance of batteries with in situ CPE at 90 °C.

overpotential at 60 °C is slightly higher than that at 90 °C, which can be attributed to the decreased ionic conductivity and slower Li^+ transport kinetics at 60 °C.

To better illustrate the improvement, comparison on rate capability of ceramic-free SPE, ex situ CPE, and in situ CPE is shown in Figure 4c. The rate was set at 1 C and temperature at 90 °C. It is evident that huge rate capacity improvement can be obtained with in situ CPE. The capacity retention of in situ CPE almost doubles the value of the ex situ counterpart, with ~120 mAh g^{-1} and ~65 mAh g^{-1}, respectively. It is noted that the ceramic-free CPE shows much lower capacity retention of ~50 mAh g^{-1} with much higher overpotential, illustrating the sluggish Li^+ transport kinetics. More comprehensive rate capability tests on ceramic-free SPE and ex situ PEO-$MUSiO_2$ CPE are shown in Supplementary Figure S7. When compared with that of in situ CPE in Figure 4a, considerable enhancement on capacity retention for in situ CPE can be observed at different rates.

Stable cycle performance of in situ PEO-$MUSiO_2$ CPE can also be observed (Figure 4d). After 80 cycles, >105 mAh g^{-1} of specific capacity can still be retained, which is a powerful indicator of the stable operation of the CPE at elevated temperature. In addition, no internal short circuit caused by Li dendrite formation was observed during the cycling. This indicates the good mechanical strength of the CPE with in situ synthesized SiO_2. It is noted that the capacity slightly decreases after cycles. This might be attributed to the unstable interface on Li metal side. Due to the huge volume change of Li and the formation of mossy Li dendrite, the solid electrolyte interphase can accumulate and affect ion transfer process.[27,28,67] Since there is no obvious increase in overpotential (Supplementary Figure S8), we can conclude that the ionic conductivity of CPE does not change much with time.

The demonstration of LFP/CPE/Li cell is a good indication of the improved electrochemical performance of CPE. The decrease of the overpotential at different C-rate and the enhanced capacity retention at high rate further confirm the improved ionic conductivity of in situ CPE. The relatively stable cycling supports the good electrochemical stability of our CPE within the voltage window.

In summary, we developed the in situ hydrolysis method for the synthesis of PEO-$MUSiO_2$ CPE. With well-controlled hydrolysis, precise SiO_2 sizes with high monodispersity can be obtained. This method not only provides much stronger PEO-SiO_2 interactions by chemical bonding and mechanical wrapping but also enables better distribution of SiO_2 in PEO matrix, which further improves the effective surface area for Lewis acid−base interaction. With the advantages, much lower degree of crystallinity and much higher degree of $LiClO_4$ dissociation in PEO can be obtained simultaneously in CPE, both of which are crucial for high ionic conductivity. As a consequence, high ionic conductivity of 4.4×10^{-5} S cm^{-1} can be achieved at 30 °C and 1.2×10^{-3} S cm^{-1} can be attained at elevated temperature of 60 °C. In addition, considerably improved electrochemical stability is realized with in situ CPE, which can endure up to 5.5 V versus Li^+/Li without significant anodic decomposition. Moreover, the in situ CPE with high ionic conductivity and electrochemical stability enables the fabrication of all-solid-state Li batteries with appreciably enhanced performance. The capacity retention at 1C reaches ~120 mAh g^{-1} and ~100 mAh g^{-1} at 90 and 60 °C, respectively. This opens up an opportunity to develop SPE with highly improved ionic conductivity and good electrochemical stability for next generation high-energy, safe Li batteries.

Methods. *Solid Electrolyte Synthesis.* For in situ CPEs synthesis (~12 nm), 1.2 g of PEO (Aldrich, average M_v ~ 600 000) was dissolved in 50 mL of deionized (DI) water. The pH of the solution was adjusted to be ~10.4 with $NH_3 \cdot H_2O$ (Sigma). To the solution, TEOS (0.54 g, Sigma) was added dropwise to initiate the hydrolysis reaction. The resultant

DOI: 10.1021/acs.nanolett.5b04117
Nano Lett. 2016, 16, 459−465

biphase system was stirred with an one-inch stir bar at 600 rpm for 24 h, and the temperature was kept constantly at 60 °C in mineral oil bath. After the reaction was complete, 0.36 g of dehydrated $LiClO_4$ was added to the solution. The water in solution was partially evaporated to obtain solution with adequate viscosity. ~200 μm in average of final CPE films were made by doctor blading on PTFE patch dishes. The as-obtained films were kept in vacuum oven at 60 °C for 24 h to completely remove the solvent. They were then transferred into an argon-filled glovebox (O_2 and H_2O at subppm value, typically <0.6 ppm) and stored for at least 48 h before measurement to remove the trace amount of water. The CPEs were stored in the glovebox for later measurement. In situ CPEs with other SiO_2 sizes were synthesized by regrowth technique with 12 nm SiO_2 as seed. The detailed synthetic procedures of other samples are included in Supporting Information.

Characterizations. TEM images were taken using either a FEI Tecnai G2 F20 X-TWIN TEM or a FEI Titan 80-300 environmental TEM. The SEM images were taken either with FEI XL30 Sirion SEM or FEI Magellan 400 XHR SEM. The FT-IR spectra were measured with a Nicolet iS50 FT-IR Spectrometer. The XRD patterns were obtained on a PANalytical X'Pert, Ni-filtered Cu Kα radiation.

Electrochemical Measurements. $LiFePO_4$ powders (MTI Inc.) and carbon black (Super P, TIMCAL, Switzerland) were first dried in vacuum oven for 24 h to remove trapped water. PEO-$LiClO_4$ SPE dissolved in acetonitrile was used as binder here. To prepare the $LiFePO_4$ electrode, slurries containing $LiFePO_4$ powders, PEO-$LiClO_4$ SPE and carbon black in ratio of 65:20:15 was dispersed in acetonitrile (Sigma). The slurries were then uniformly coated on Al foils. The mass loading is controlled to be ~1.0 mg cm^{-2} for the study. For ionic conductivity measurement, symmetric SS/SPE/SS cells were assembled, while for electrochemical stability measurement lithium/SPE/SS cells were assembled. A surface of stainless steel is coated with 250 nm Pt using e-beam evaporation. For all-solid-state batteries, SPEs were sandwiched between lithium metal foils and $LiFePO_4$ electrodes to form cells. Electrochemical measurements were carried out on a Biologic VMP3 system. The temperature of the cells was controlled by an environmental chamber (BTU-133, ESPEC North America, Inc.), while the precision of the thermometer is ±0.1 °C.

■ ASSOCIATED CONTENT

Supporting Information

The Supporting Information is available free of charge on the ACS Publications website at DOI: 10.1021/acs.nanolett.5b04117.

Detailed synthetic procedures, SEM images of SiO_2 nanospheres with different sizes, FT-IR and DSC spectra of the solid polymer electrolytes, TEM images of the ex situ PEO−SiO_2 composite, SEM images of the in situ CPE, as well as supplementary electrochemical characterizations (PDF)

■ AUTHOR INFORMATION

Corresponding Author

*E-mail: yicui@stanford.edu.

Author Contributions

D.L. and Y.C. conceived the concept and designed the experiments. D.L. conducted the synthesis, most of the characterizations and the electrochemical measurement. Y.L. and P.-C.H. contribute to the characterizations. W.L. and H.R.L performed the TEM characterization. D.L. and Y.C. cowrote the paper. All authors discussed the results and commented on the manuscript.

Notes

The authors declare no competing financial interest.

■ REFERENCES

(1) Tarascon, J. M.; Armand, M. *Nature* **2001**, *414* (6861), 359−367.
(2) Armand, M.; Tarascon, J. M. *Nature* **2008**, *451* (7179), 652−657.
(3) Xu, K. *Chem. Rev.* **2004**, *104* (10), 4303−4418.
(4) Xu, K. *Chem. Rev.* **2014**, *114* (23), 11503−11618.
(5) Wu, H.; Chan, G.; Choi, J. W.; Ryu, I.; Yao, Y.; McDowell, M. T.; Lee, S. W.; Jackson, A.; Yang, Y.; Hu, L.; Cui, Y. *Nat. Nanotechnol.* **2012**, *7* (5), 310−315.
(6) Liu, N.; Lu, Z.; Zhao, J.; McDowell, M. T.; Lee, H.-W.; Zhao, W.; Cui, Y. *Nat. Nanotechnol.* **2014**, *9* (3), 187−192.
(7) Lin, D.; Lu, Z.; Hsu, P.-C.; Lee, H. R.; Liu, N.; Zhao, J.; Wang, H.; Liu, C.; Cui, Y. *Energy Environ. Sci.* **2015**, *8* (8), 2371−2376.
(8) Ding, F.; Xu, W.; Graff, G. L.; Zhang, J.; Sushko, M. L.; Chen, X.; Shao, Y.; Engelhard, M. H.; Nie, Z.; Xiao, J.; Liu, X.; Sushko, P. V.; Liu, J.; Zhang, J.-G. *J. Am. Chem. Soc.* **2013**, *135* (11), 4450−4456.
(9) Zheng, G.; Lee, S. W.; Liang, Z.; Lee, H.-W.; Yan, K.; Yao, H.; Wang, H.; Li, W.; Chu, S.; Cui, Y. *Nat. Nanotechnol.* **2014**, *9* (8), 618−623.
(10) Yan, K.; Lee, H.-W.; Gao, T.; Zheng, G.; Yao, H.; Wang, H.; Lu, Z.; Zhou, Y.; Liang, Z.; Liu, Z.; Chu, S.; Cui, Y. *Nano Lett.* **2014**, *14* (10), 6016−6022.
(11) Qian, J.; Henderson, W. A.; Xu, W.; Bhattacharya, P.; Engelhard, M.; Borodin, O.; Zhang, J.-G. *Nat. Commun.* **2015**, *6*, 6362.
(12) Sun, Y.-K.; Myung, S.-T.; Park, B.-C.; Prakash, J.; Belharouak, I.; Amine, K. *Nat. Mater.* **2009**, *8* (4), 320−324.
(13) Ji, X.; Lee, K. T.; Nazar, L. F. *Nat. Mater.* **2009**, *8* (6), 500−506.
(14) Wei Seh, Z.; Li, W.; Cha, J. J.; Zheng, G.; Yang, Y.; McDowell, M. T.; Hsu, P.-C.; Cui, Y. *Nat. Commun.* **2013**, *4*, 1331.
(15) Croce, F.; Appetecchi, G. B.; Persi, L.; Scrosati, B. *Nature* **1998**, *394* (6692), 456−458.
(16) Gadjourova, Z.; Andreev, Y. G.; Tunstall, D. P.; Bruce, P. G. *Nature* **2001**, *412* (6846), 520−523.
(17) Wright, P. V. *Br. Polym. J.* **1975**, *7* (5), 319−327.
(18) Berthier, C.; Gorecki, W.; Minier, M.; Armand, M. B.; Chabagno, J. M.; Rigaud, P. *Solid State Ionics* **1983**, *11* (1), 91−95.
(19) Armand, M. *Solid State Ionics* **1983**, *9−10*, 745−754.
(20) Bates, J. B.; Dudney, N. J.; Neudecker, B.; Ueda, A.; Evans, C. D. *Solid State Ionics* **2000**, *135* (1−4), 33−45.
(21) Kanno, R.; Murayama, M. *J. Electrochem. Soc.* **2001**, *148* (7), A742−A746.
(22) Kamaya, N.; Homma, K.; Yamakawa, Y.; Hirayama, M.; Kanno, R.; Yonemura, M.; Kamiyama, T.; Kato, Y.; Hama, S.; Kawamoto, K.; Mitsui, A. *Nat. Mater.* **2011**, *10* (9), 682−686.
(23) Thangadurai, V.; Weppner, W. *J. Am. Ceram. Soc.* **2005**, *88* (2), 411−418.
(24) Murugan, R.; Thangadurai, V.; Weppner, W. *Angew. Chem., Int. Ed.* **2007**, *46* (41), 7778−7781.
(25) Bohnke, O. *Solid State Ionics* **2008**, *179* (1−6), 9−15.
(26) Stone, G. M.; Mullin, S. A.; Teran, A. A.; Hallinan, D. T.; Minor, A. M.; Hexemer, A.; Balsara, N. P. *J. Electrochem. Soc.* **2012**, *159* (3), A222−A227.
(27) Osaka, T.; Homma, T.; Momma, T.; Yarimizu, H. *J. Electroanal. Chem.* **1997**, *421* (1−2), 153−156.
(28) Harry, K. J.; Hallinan, D. T.; Parkinson, D. Y.; MacDowell, A. A.; Balsara, N. P. *Nat. Mater.* **2013**, *13* (1), 69−73.
(29) Hallinan, D. T.; Balsara, N. P. *Annu. Rev. Mater. Res.* **2013**, *43* (1), 503−525.
(30) Manuel Stephan, A. *Eur. Polym. J.* **2006**, *42* (1), 21−42.
(31) Cao, J.; Wang, L.; He, X.; Fang, M.; Gao, J.; Li, J.; Deng, L.; Chen, H.; Tian, G.; Wang, J.; Fan, S. *J. Mater. Chem. A* **2013**, *1* (19), 5955−5961.

DOI: 10.1021/acs.nanolett.5b04117
Nano Lett. 2016, 16, 459−465

(32) Wang, Q.; Song, W.-L.; Fan, L.-Z.; Shi, Q. *J. Power Sources* **2015**, *279*, 405−412.
(33) Ryou, M.-H.; Lee, Y. M.; Cho, K. Y.; Han, G.-B.; Lee, J.-N.; Lee, D. J.; Choi, J. W.; Park, J.-K. *Electrochim. Acta* **2012**, *60*, 23−30.
(34) Singh, M.; Odusanya, O.; Wilmes, G. M.; Eitouni, H. B.; Gomez, E. D.; Patel, A. J.; Chen, V. L.; Park, M. J.; Fragouli, P.; Iatrou, H.; Hadjichristidis, N.; Cookson, D.; Balsara, N. P. *Macromolecules* **2007**, *40* (13), 4578−4585.
(35) Wanakule, N. S.; Panday, A.; Mullin, S. A.; Gann, E.; Hexemer, A.; Balsara, N. P. *Macromolecules* **2009**, *42* (15), 5642−5651.
(36) Gomez, E. D.; Panday, A.; Feng, E. H.; Chen, V.; Stone, G. M.; Minor, A. M.; Kisielowski, C.; Downing, K. H.; Borodin, O.; Smith, G. D.; Balsara, N. P. *Nano Lett.* **2009**, *9* (3), 1212−1216.
(37) Choi, I.; Ahn, H.; Park, M. J. *Macromolecules* **2011**, *44* (18), 7327−7334.
(38) Bouchet, R.; Maria, S.; Meziane, R.; Aboulaich, A.; Lienafa, L.; Bonnet, J.-P.; Phan, T. N. T.; Bertin, D.; Gigmes, D.; Devaux, D.; Denoyel, R.; Armand, M. *Nat. Mater.* **2013**, *12* (5), 452−457.
(39) Sun, J.; Liao, X.; Minor, A. M.; Balsara, N. P.; Zuckermann, R. N. *J. Am. Chem. Soc.* **2014**, *136* (42), 14990−14997.
(40) Wright, P. V.; Zheng, Y.; Bhatt, D.; Richardson, T.; Ungar, G. *Polym. Int.* **1998**, *47* (1), 34−42.
(41) Chung, S. H.; Wang, Y.; Greenbaum, S. G.; Golodnitsky, D.; Peled, E. *Electrochem. Solid-State Lett.* **1999**, *2* (11), 553−555.
(42) Yang, L.-Y.; Wei, D.-X.; Xu, M.; Yao, Y.-F.; Chen, Q. *Angew. Chem.* **2014**, *126* (14), 3705−3709.
(43) Depre, L.; Kappel, J.; Popall, M. *Electrochim. Acta* **1998**, *43* (10−11), 1301−1306.
(44) Honma, I.; Hirakawa, S.; Yamada, K.; Bae, J. M. *Solid State Ionics* **1999**, *118* (1−2), 29−36.
(45) Gupta, R. K.; Jung, H. Y.; Whang, C. M. *J. Mater. Chem.* **2002**, *12* (12), 3779−3782.
(46) Wieczorek, W.; Raducha, D.; Zalewska, A.; Stevens, J. R. *J. Phys. Chem. B* **1998**, *102* (44), 8725−8731.
(47) Scrosati, B.; Croce, F.; Persi, L. *J. Electrochem. Soc.* **2000**, *147* (5), 1718−1721.
(48) Scrosati, B.; Croce, F.; Panero, S. *J. Power Sources* **2001**, *100* (1−2), 93−100.
(49) Croce, F.; Persi, L.; Scrosati, B.; Serraino-Fiory, F.; Plichta, E.; Hendrickson, M. A. *Electrochim. Acta* **2001**, *46* (16), 2457−2461.
(50) Chen-Yang, Y. W.; Chen, Y. T.; Chen, H. C.; Lin, W. T.; Tsai, C. H. *Polymer* **2009**, *50* (13), 2856−2862.
(51) Tang, C.; Hackenberg, K.; Fu, Q.; Ajayan, P. M.; Ardebili, H. *Nano Lett.* **2012**, *12* (3), 1152−1156.
(52) Gurevitch, I.; Buonsanti, R.; Teran, A. A.; Gludovatz, B.; Ritchie, R. O.; Cabana, J.; Balsara, N. P. *J. Electrochem. Soc.* **2013**, *160* (9), A1611−A1617.
(53) Zhu, Z.; Hong, M.; Guo, D.; Shi, J.; Tao, Z.; Chen, J. *J. Am. Chem. Soc.* **2014**, *136* (47), 16461−16464.
(54) Gowneni, S.; Ramanjaneyulu, K.; Basak, P. *ACS Nano* **2014**, *8* (11), 11409−11424.
(55) Wieczorek, W.; Stevens, J. R.; Florjańczyk, Z. *Solid State Ionics* **1996**, *85* (1−4), 67−72.
(56) Marcinek, M.; Bac, A.; Lipka, P.; Zalewska, A.; Żukowska, G.; Borkowska, R.; Wieczorek, W. *J. Phys. Chem. B* **2000**, *104* (47), 11088−11093.
(57) Yokoi, T.; Sakamoto, Y.; Terasaki, O.; Kubota, Y.; Okubo, T.; Tatsumi, T. *J. Am. Chem. Soc.* **2006**, *128* (42), 13664−13665.
(58) Wang, J.; Sugawara-Narutaki, A.; Fukao, M.; Yokoi, T.; Shimojima, A.; Okubo, T. *ACS Appl. Mater. Interfaces* **2011**, *3* (5), 1538−1544.
(59) Hartlen, K. D.; Athanasopoulos, A. P. T.; Kitaev, V. *Langmuir* **2008**, *24* (5), 1714−1720.
(60) Salomon, M.; Xu, M.; Eyring, E. M.; Petrucci, S. *J. Phys. Chem.* **1994**, *98* (33), 8234−8244.
(61) Xiong, H.-M.; Zhao, X.; Chen, J.-S. *J. Phys. Chem. B* **2001**, *105* (42), 10169−10174.
(62) Wang, X.-L.; Fan, L.-Z.; Mei, A.; Ma, F.-Y.; Lin, Y.-H.; Nan, C.-W. *Electrochim. Acta* **2008**, *53* (5), 2448−2452.
(63) Park, C. H.; Kim, D. W.; Prakash, J.; Sun, Y.-K. *Solid State Ionics* **2003**, *159* (1−2), 111−119.
(64) Croce, F.; Sacchetti, S.; Scrosati, B. *J. Power Sources* **2006**, *162* (1), 685−689.
(65) Hallinan, D. T.; Mullin, S. A.; Stone, G. M.; Balsara, N. P. *J. Electrochem. Soc.* **2013**, *160* (3), A464−A470.
(66) Soo, P. P.; Huang, B.; Jang, Y. I.; Chiang, Y. M.; Sadoway, D. R.; Mayes, A. M. *J. Electrochem. Soc.* **1999**, *146* (1), 32−37.
(67) Peled, E.; Golodnitsky, D.; Ardel, G. *J. Electrochem. Soc.* **1997**, *144* (8), L208−L210.

DOI: 10.1021/acs.nanolett.5b04117
Nano Lett. 2016, 16, 459−465